Supporting Information

Luminescent sensing and photocatalytic degradation properties of an uncommon (4,5,5)-connected 3D MOF based on 3,5-di(3′, 5′-dicarboxylphenyl)benzoic acid: an experimental and computational study

Jun-Cheng Jin[#a], Xi-Ren Wu[#b], Zhi-Dong Luo[b], Fang-Yuan Deng,[a] Jian-Qiang Liu[b*], Amita Singh[c] and Abhinav Kumar[c*]

Sensing Method

The photoluminescence sensing were performed as follows: the photoluminescence properties of **1** (5.0 mg) were investigated in N,N-dimethylformamide (DMF)/H_2O emulsions at room temperature using a RF-5301PC spectrofluorophotometer. The inclusions were prepared by adding 5 mg of **1** powder into 3.00 mL of DMF/H_2O and then ultrasonic agitation the mixture for 30 min before testing.

Photocatalytic Method

The photocatalytic reactions were performed as follows: 50 mg of **1** were dispersed in 50 mL aqueous solution of MV or RhB (10 mg/L) under stirring in the dark for 30 min to ensure the establishment of an adsorption-desorption equilibrium. Then the mixed solution was exposed to UV irradiation from an Hg lamp (250 W) and kept under continuous stirring during irradiation for 100 min. Samples of 5 mL were taken out every 10 min and collected by centrifugation for analysis by UV-Vis spectrometer. By contrast, the simple control experiment was also performed under the same condition without adding any catalysts.

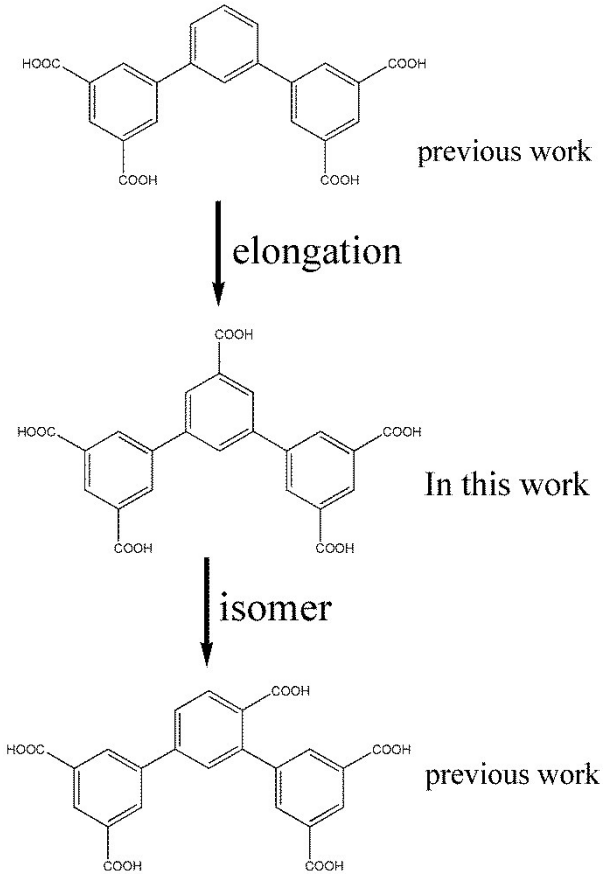

Scheme S1 the synthetic strategy and decorated ligand in this work.

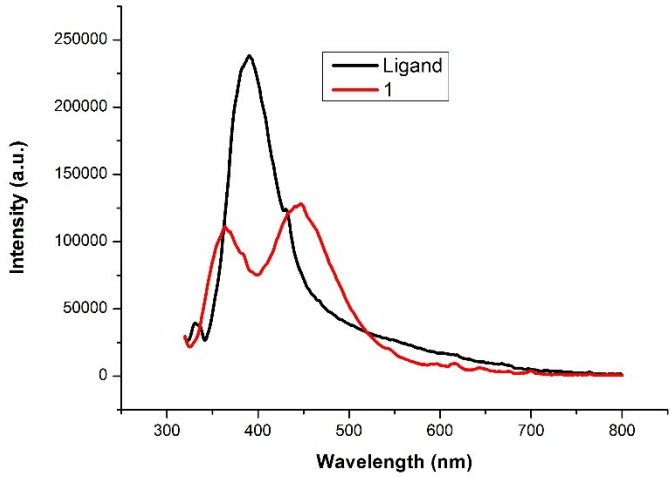

Fig. S1 view of the PL for solid state of **1** at room temperature (λ_{ex} = 321 nm).

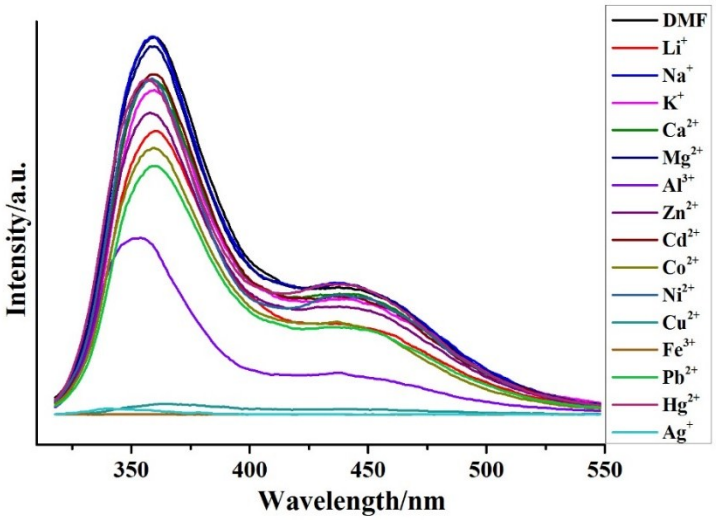

Fig. S2 Emission spectra of **1** at different metal ions concentrations in DMF.

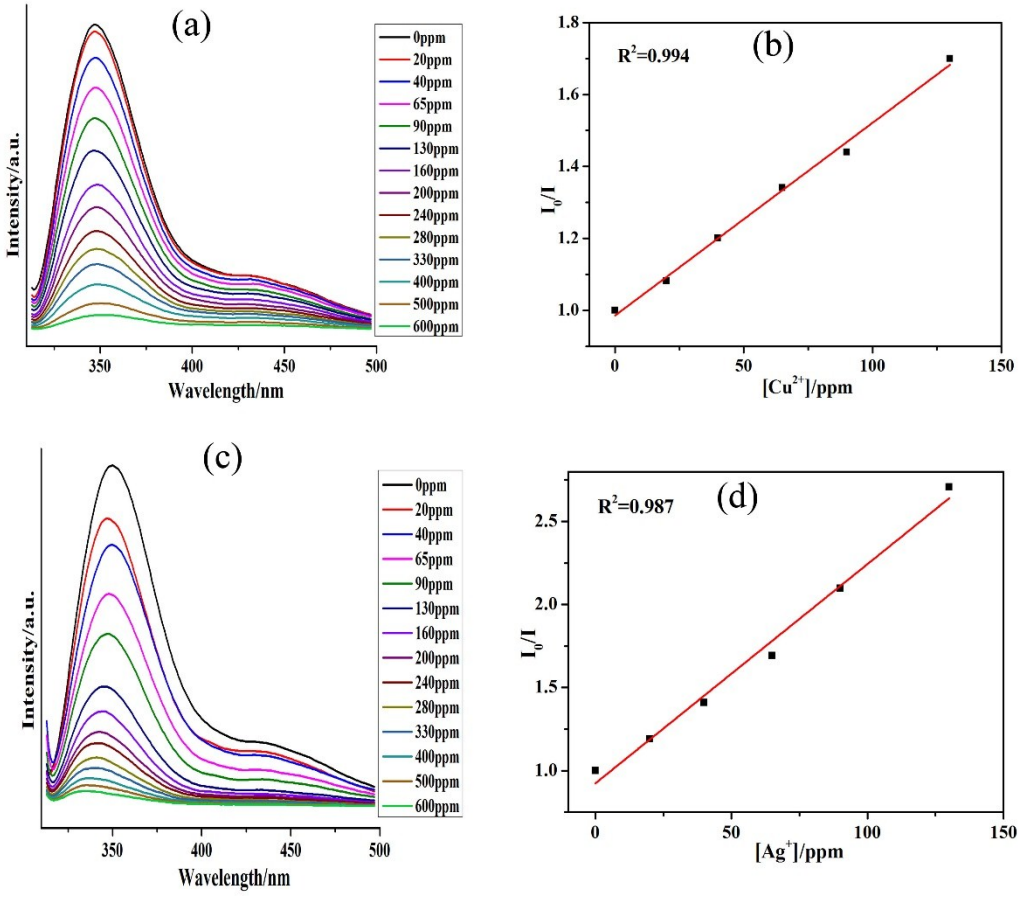

Fig. S3 (a) and (c) emissive response spectra of **1** for Cu^{2+} and Ag^{+} in DMF solution with different concentrations; (b) and (d) The Stern–Volmer plot for Cu^{2+} and Ag^{+} upon adding of 1mM.

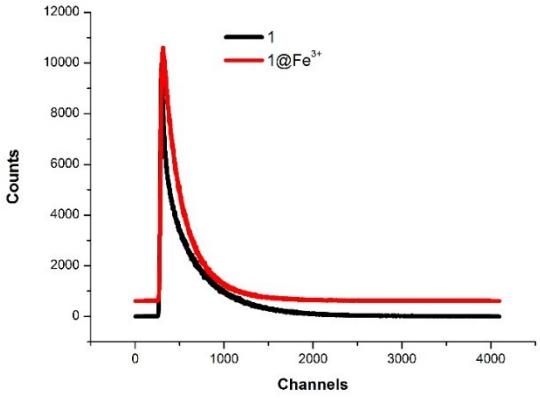

Fig. S4 Comparison of the fluorescence lifetime studies of original samples (black) and Fe^{3+}-infused **1** in 10^{-2} $Fe(NO_3)_3$ DMF solution (red).

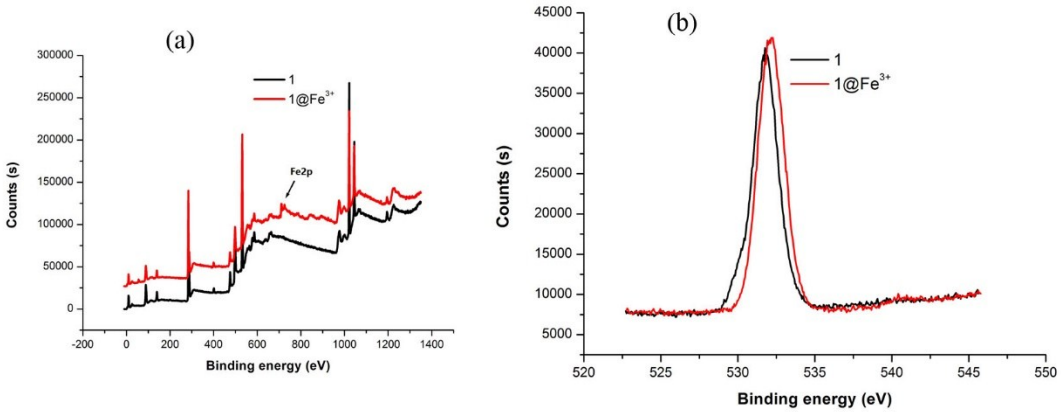

Fig. S5. (a) XPS spectra of the **1**@Fe^{3+} (red) and original **1** (black); (b) O1s XPS spectra of the original **1** (black) and **1**@Fe^{3+} (red).

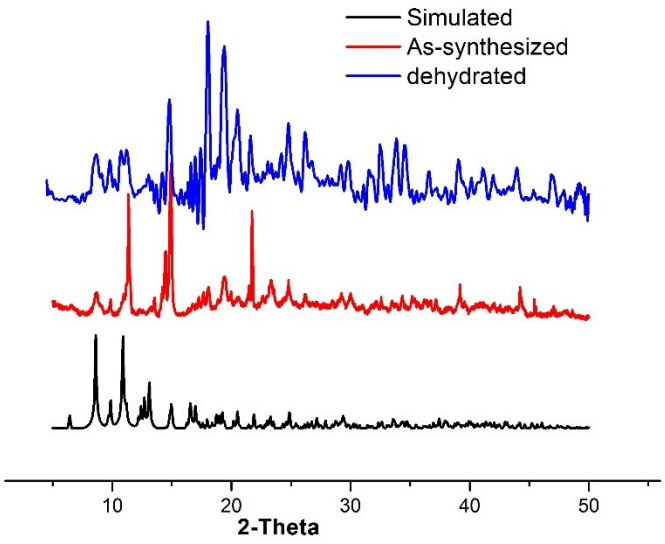

Fig. S6 view of the PXRD for the sample **1** (black: simulated; red: as-synthesized; blue: dehydrated ones).

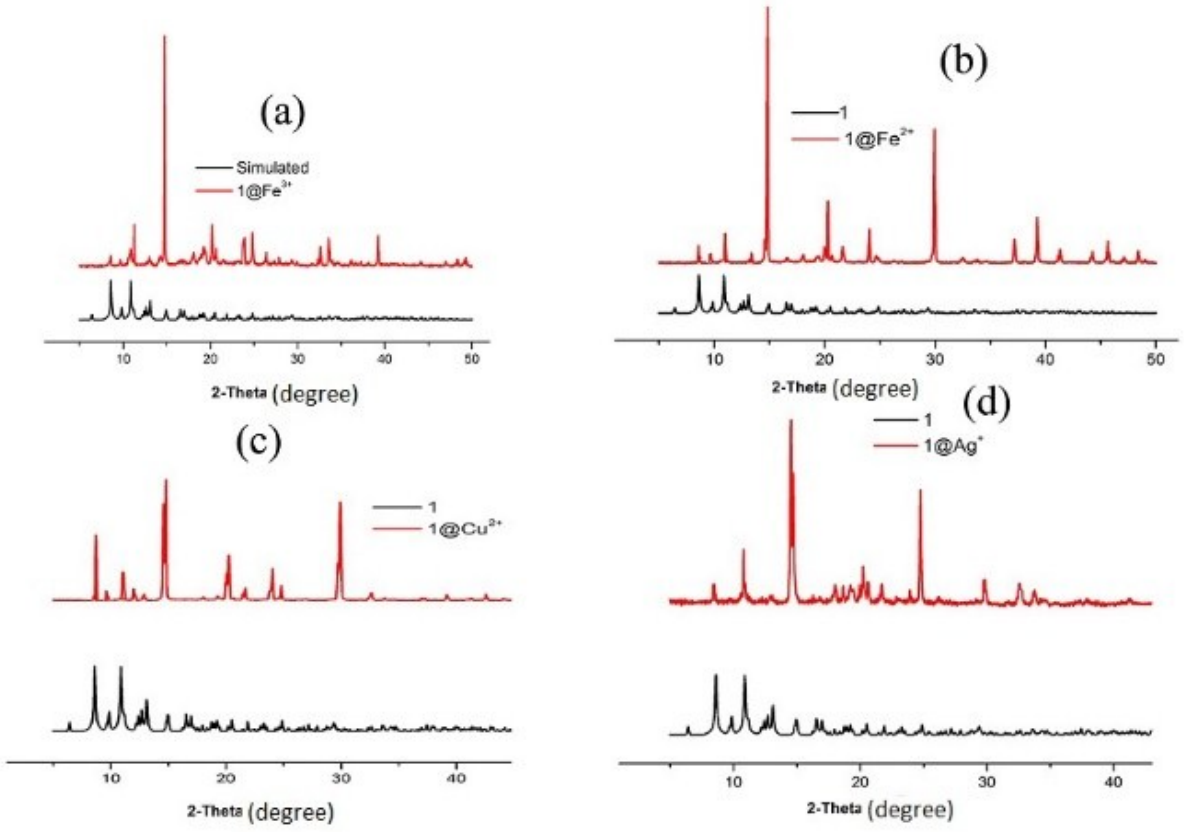

Fig. S7 view of the PXRD pattern of **1** at different metal suspension.

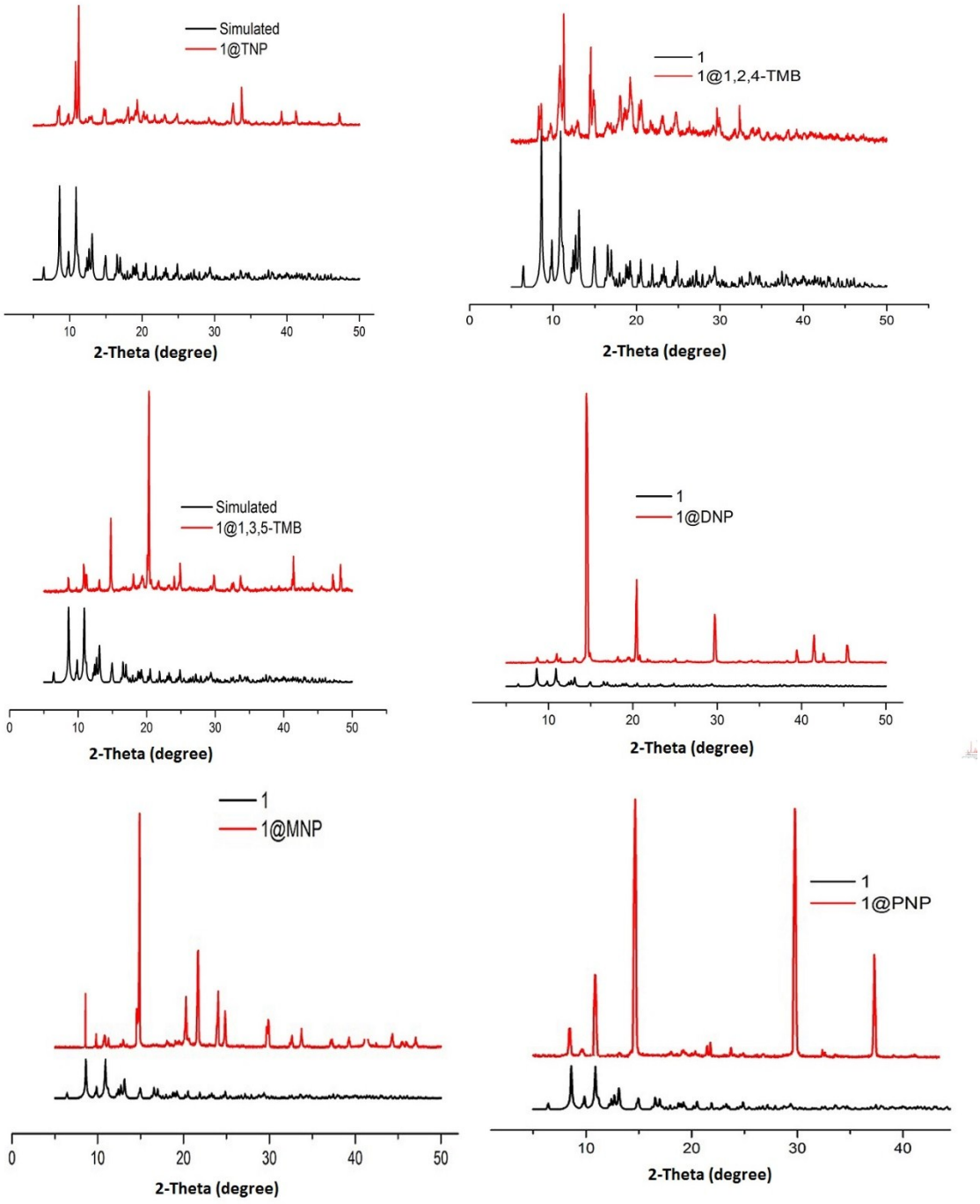

Fig. S8 view of the PXRD pattern of **1** dispersed in different explosives.

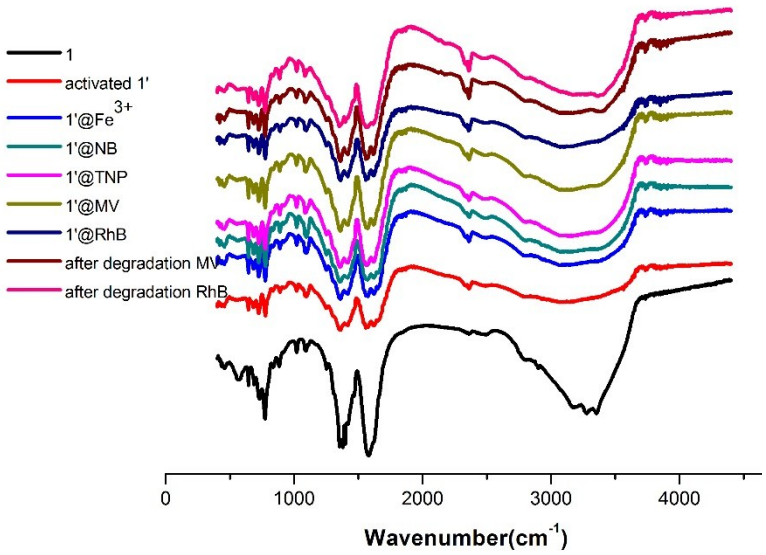

Fig. S9 view of the IR in different inclusions.

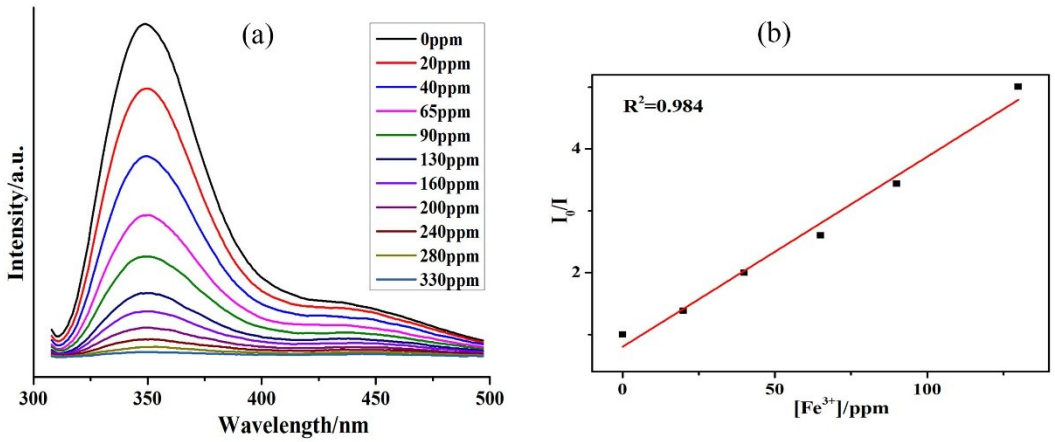

Fig. S10 (a) emissive response spectra of **1** for Fe^{3+} in water with different concentrations upon adding of 1mM; (b) and (d) The Stern–Volmer plot for Fe^{3+}.

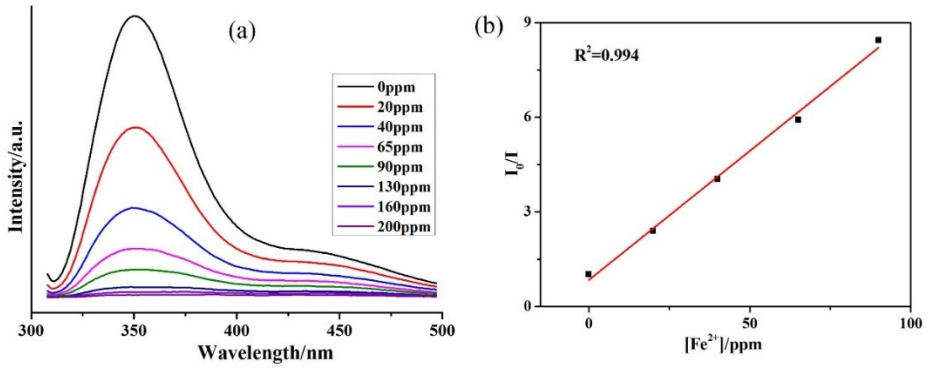

Fig. S11 (a) emissive response spectra of **1** for Fe^{2+} in water with different concentrations upon adding of 1mM; (b) and (d) The Stern–Volmer plot for Fe^{3+}.

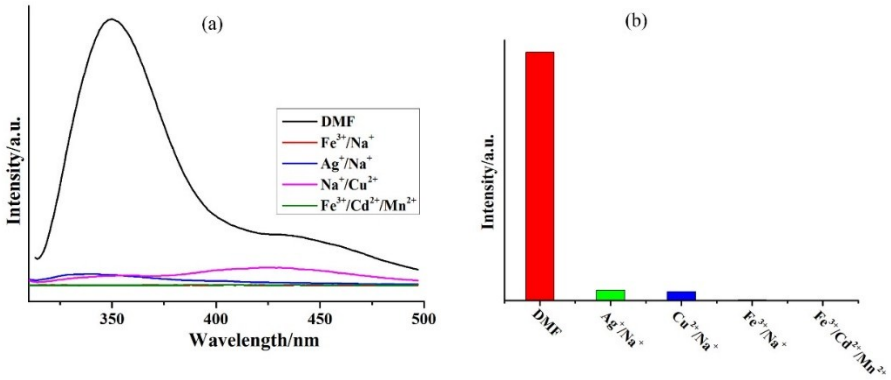

Fig. S12 (a) and (b) view of Luminescence intensity of **1** dispersed in H_2O with addition of different mixed ions (10^{-3} M).

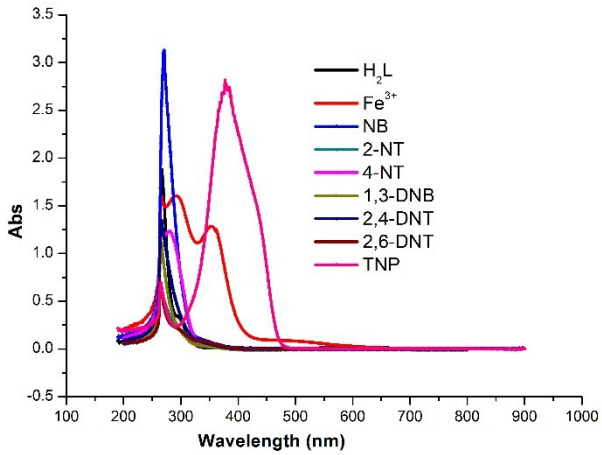

Fig. S13 view of spectra of the UV-vis for different analytes and ligand.

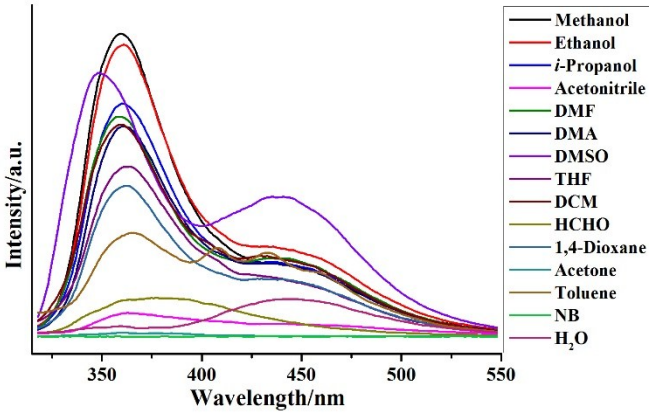

Fig. S14 Emission spectra of **1** at different solvents concentrations in DMF.

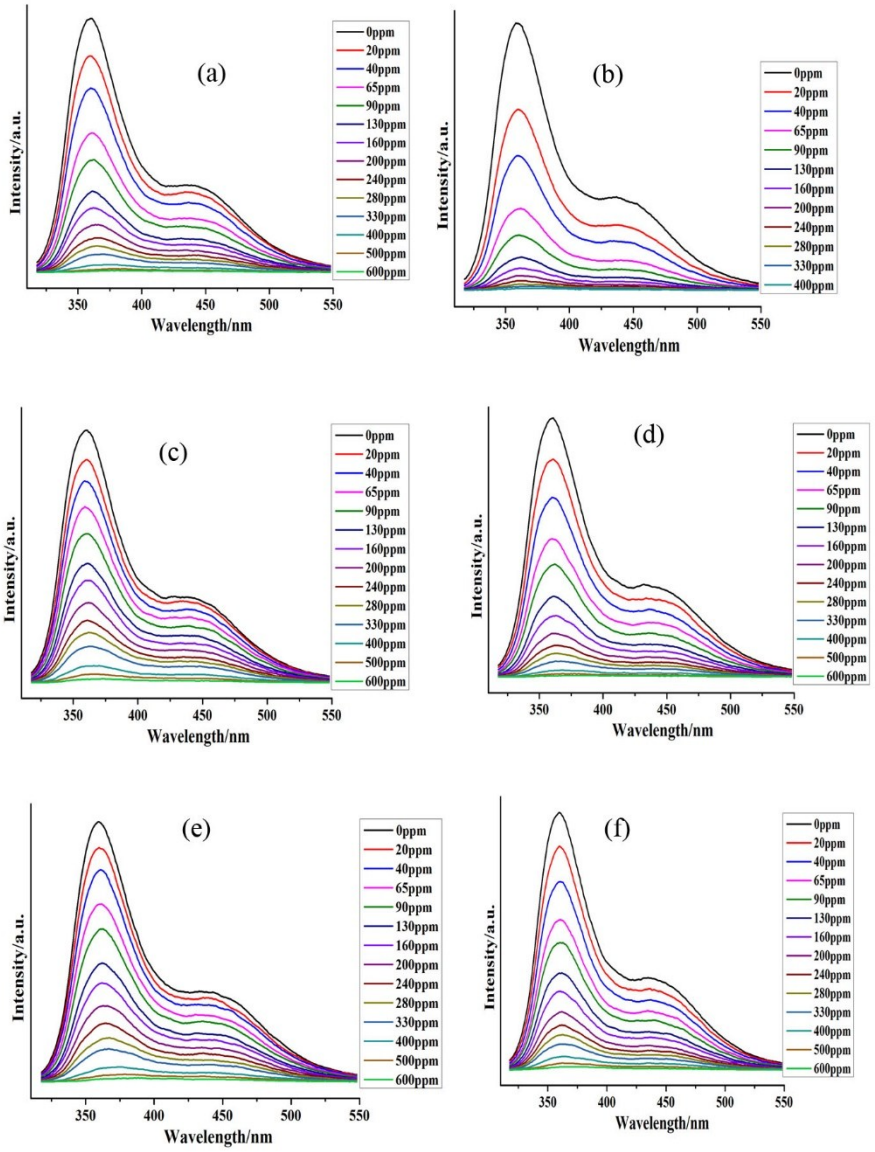

Fig. S15 (a)-(f) emissive response spectra of **1** for 2-NT, 4-NT, 1,3-DNB, 2,4-DNT, 2,6-DNT and NB in DMF solution with different concentrations, respectively.

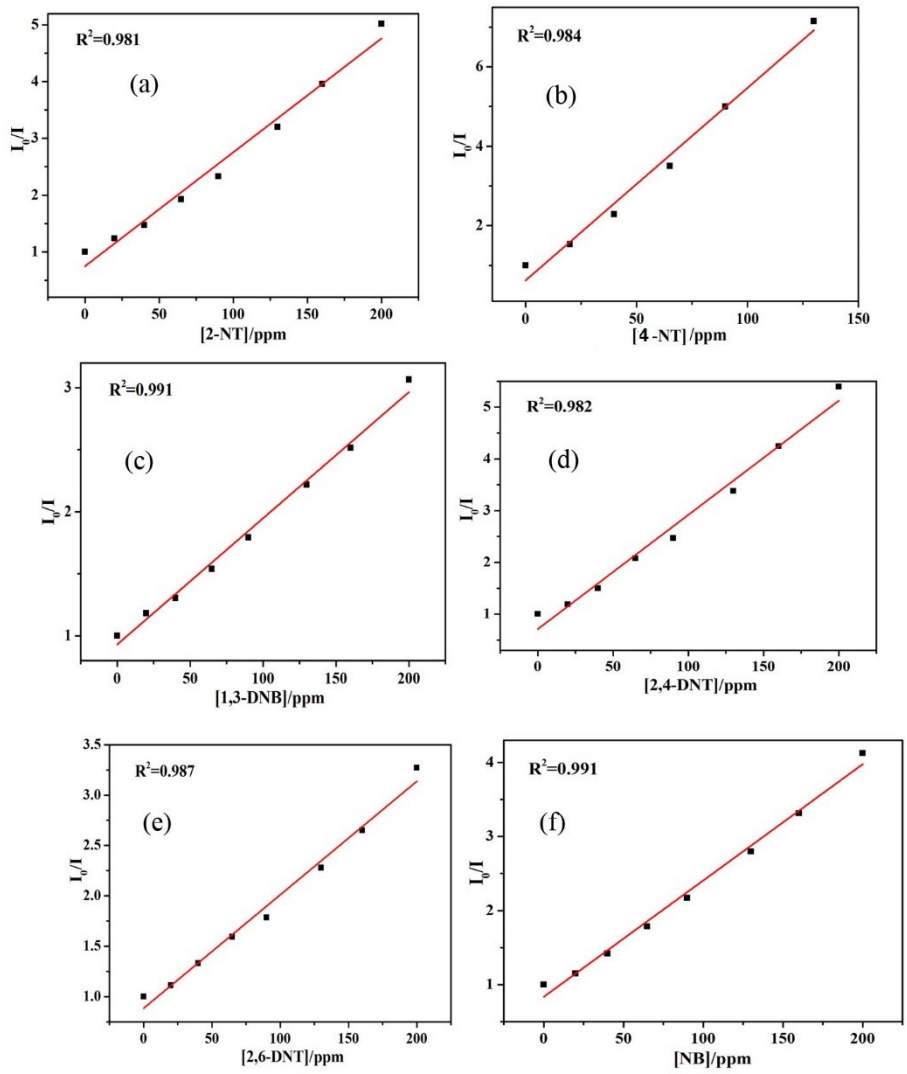

Fig. S16 (a)-(f) view of the Stern–Volmer plot for 2-NT, 4-NT, 1,3-DNB, 2,4-DNT, 2,6-DNT and NB.

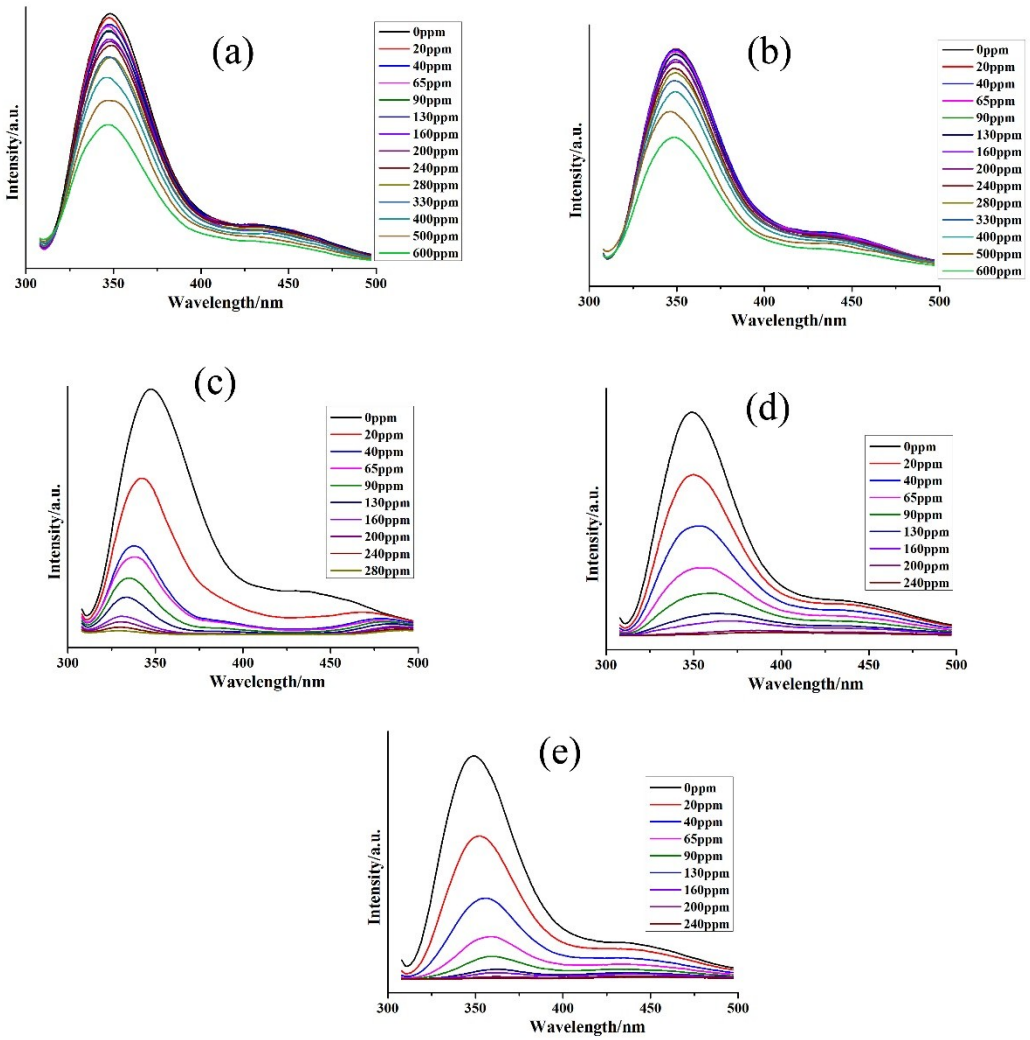

Fig. S17(a)-(e) emissive response spectra of **1** for 1,2,4-TMB, 1,3,5-TMB, MNP, PNP and DNP in DMF solution with different concentrations, respectively.

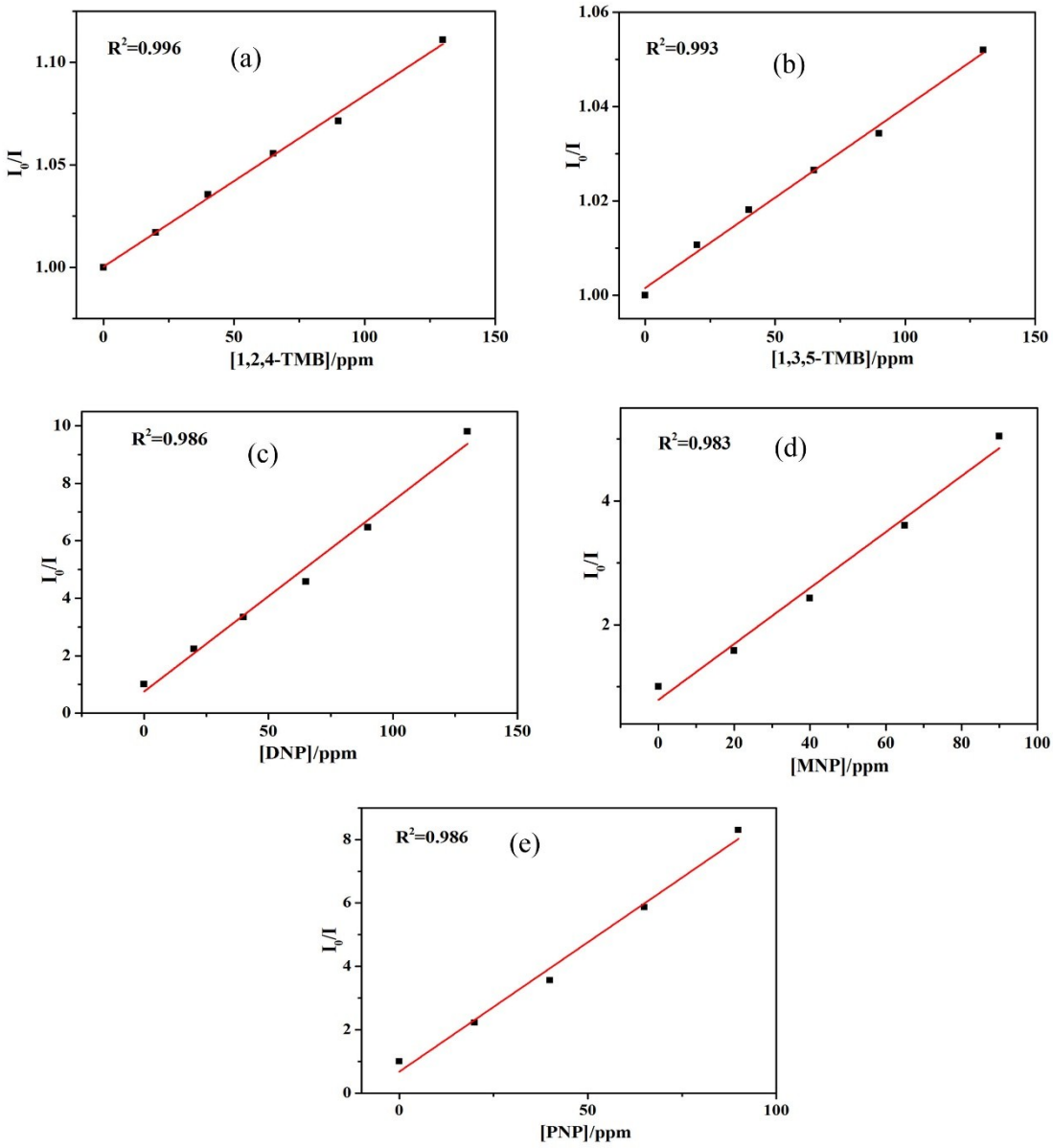

Fig. S18 (a)-(e) view of the Stern–Volmer plot for 1,2,4-TMB, 1,3,5-TMB, MNP, PNP and DNP

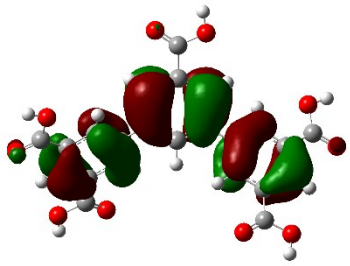 HOMO H_5L	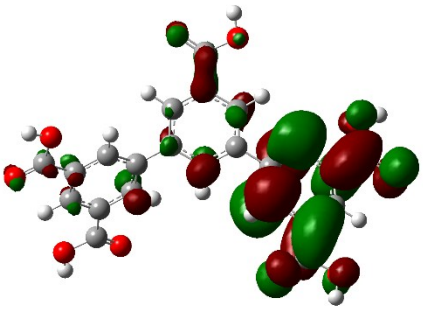 LUMO H_5L
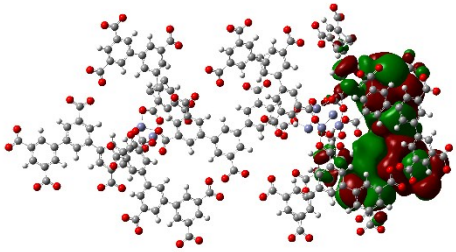 HOMO **1**	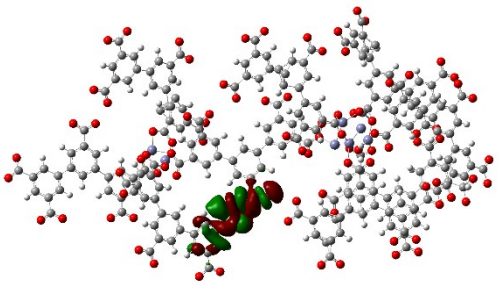 LUMO **1**
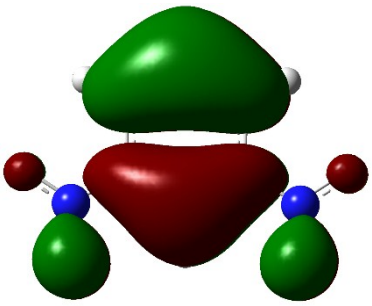 HOMO 1,3-DNB	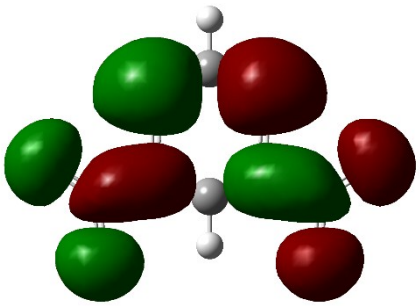 LUMO 1,3-DNB
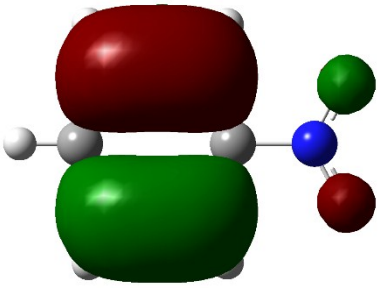 HOMO NB	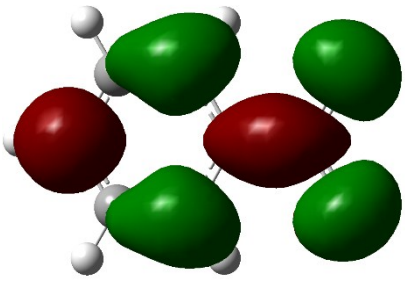 LUMO NB

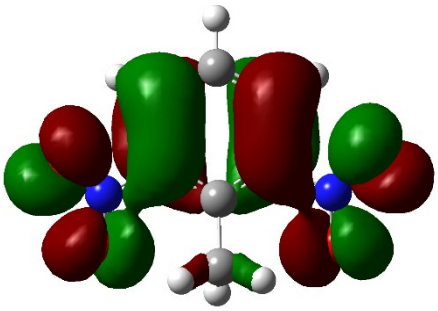 HOMO 2,6-DNT	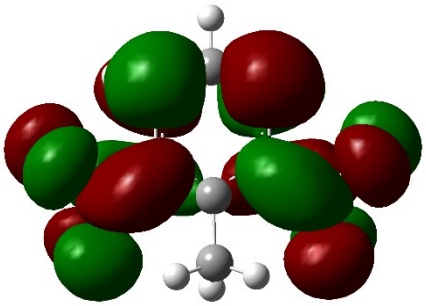 LUMO 2,6-DNT
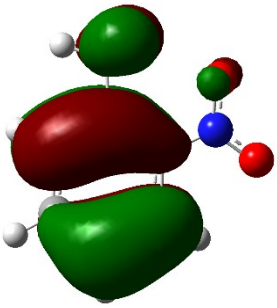 HOMO 2-NT	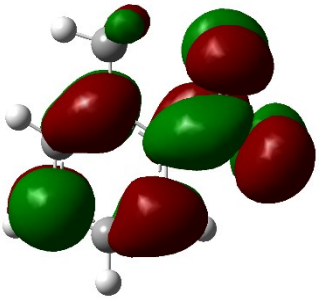 LUMO 2-NT
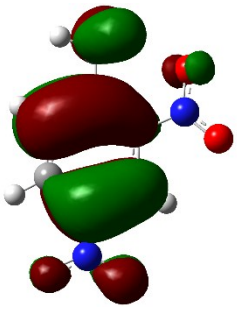 HOMO 2,4-DNT	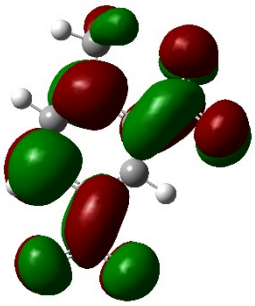 LUMO 2,4-DNT
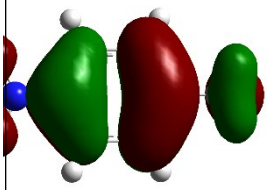 HOMO 4-NT	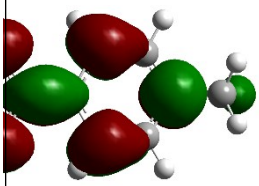 LUMO 4-NT

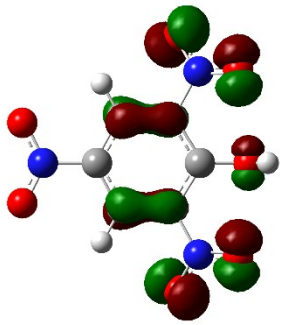 HOMO TNP	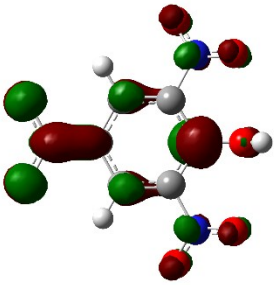 LUMO TNP
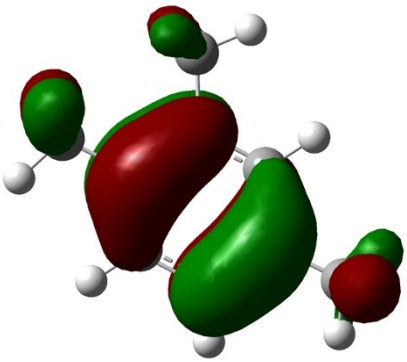 HOMO 1,2,4-TMB	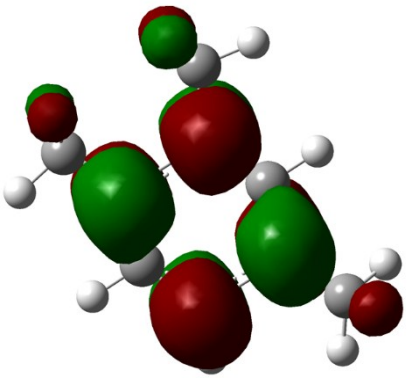 LUMO 1,2,4-TMB
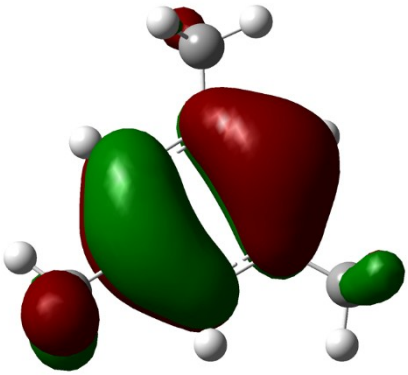 HOMO 1,3,5-TMB	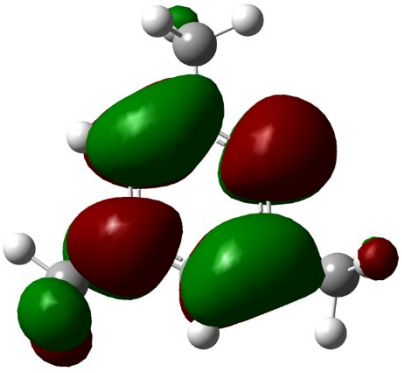 LUMO 1,3,5-TMB
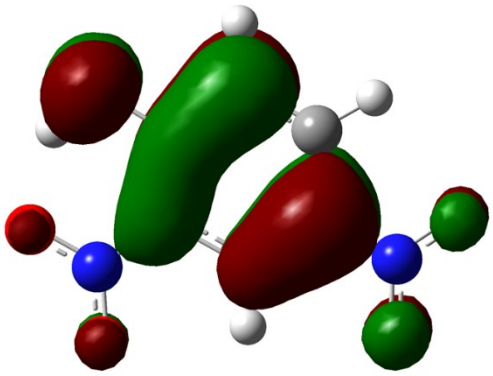 HOMO 2,4-DNP	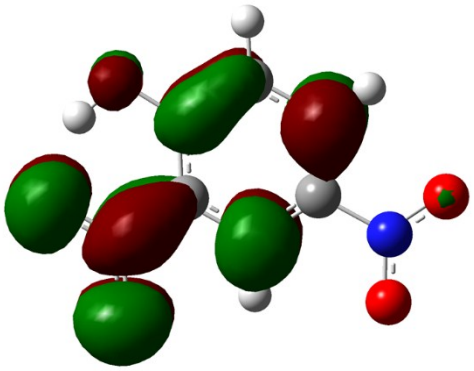 LUMO 2,4-DNP

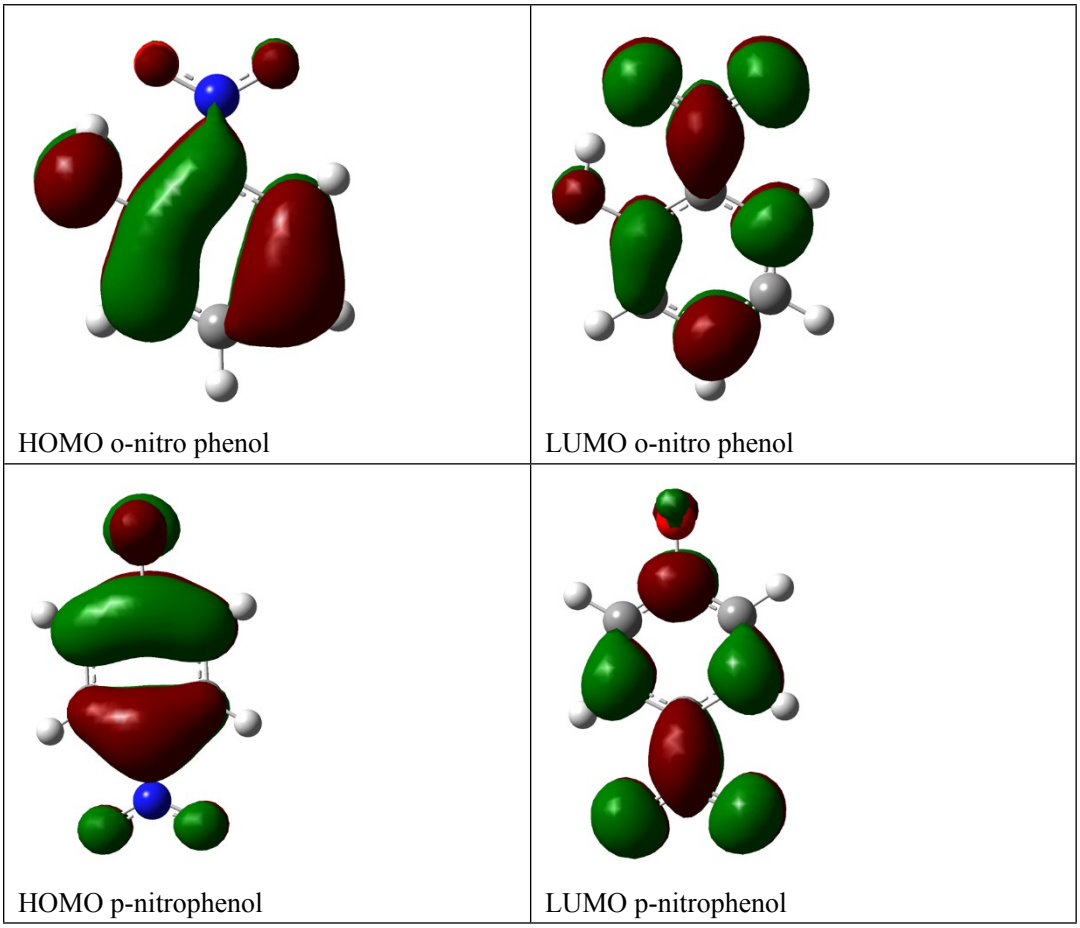

Fig. S19 HOMO–LUMO energies of the NACs along with MOF **1** and H_5L.

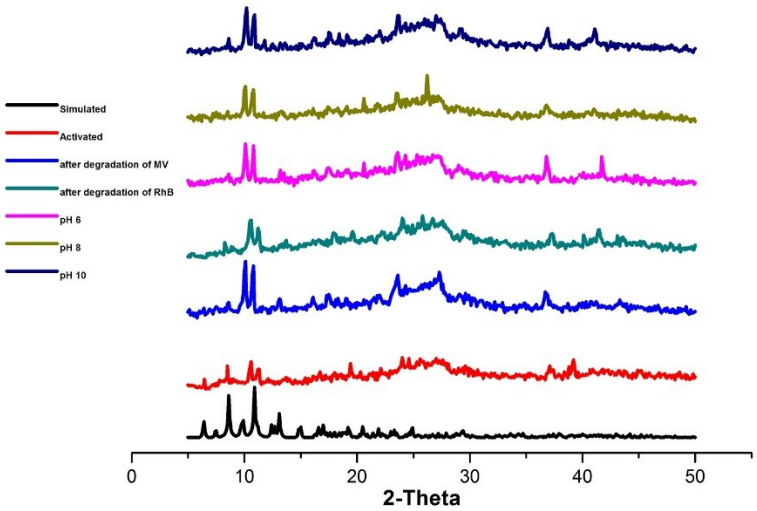

Fig. S20 PXRD profiles of **1** after photocatalysis and different pH condition.

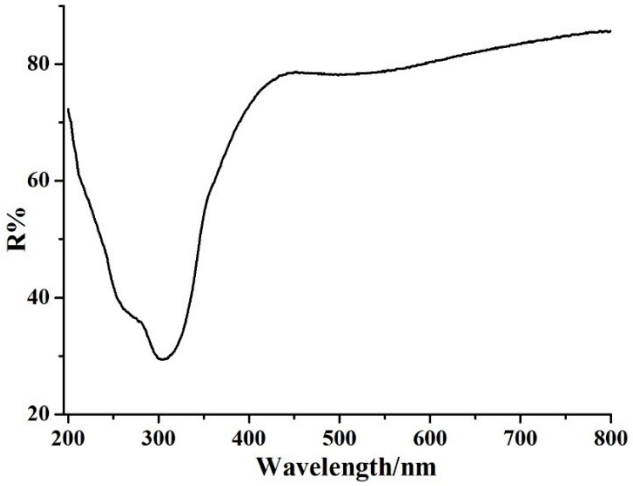

Fig. S21 view of the UV-vis-NIR.

Thermal Analysis

The thermal stabilities of crystalline samples of **1** were measured under a nitrogen atmosphere (Fig. S22). For **1**, a weight loss of 16.2 % was observed from the room temperature to 235 °C, which corresponds to the loss of coordinated water molecules, coordinated DMF and free DMF molecules (calcd. 15.5 %). Later, the decomposition of framework occurs. The final residuum is ZnO.

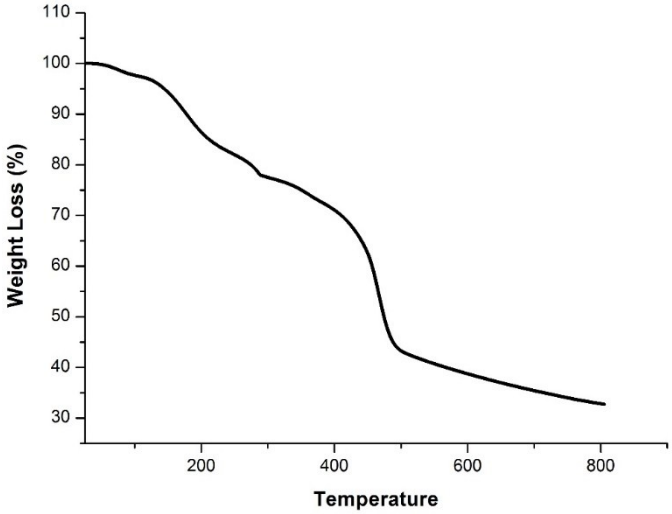

Fig. S22 view of TGA in **1**.

Measurements

The activated samples were prepared by soaking the as-synthesized samples in CH_3OH for two days, then in CH_2Cl_2 for three days and subsequent heating at 100 ºC in a quartz tube under high vacuum for 20 h to remove the solvent molecules prior to measurements. The CO_2 adsorption-desorption measurements were carried out by using automatic volumetric adsorption equipment (Micromeritics, ASAP2020).

The CO_2 sorption for **1** has been measured at 273 K and exhibits type I isotherm (Fig. S23), indicating that **1** is a microporous material with pore volume of 65.69 cm^3 (STP) g^{-1} and the BET surface area is 269.96 m^2/g.

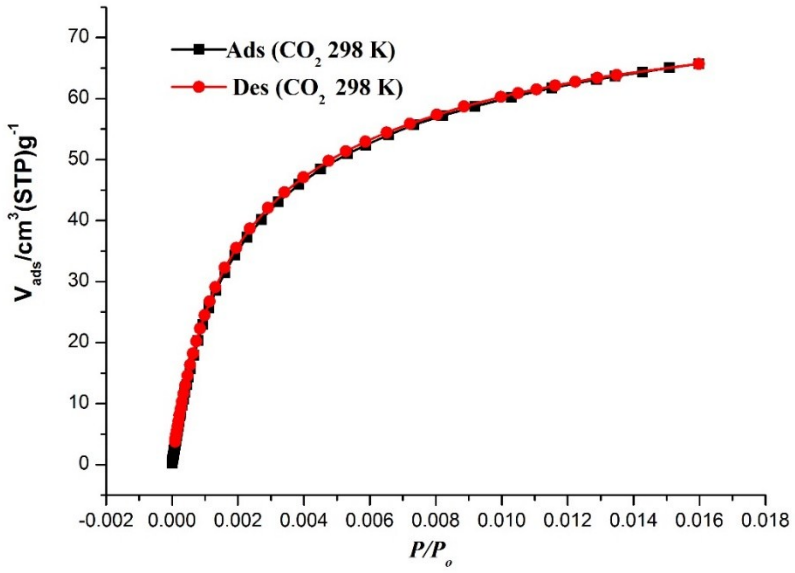

Fig. S23 view of the CO_2 adsorption isotherms at 273 K.

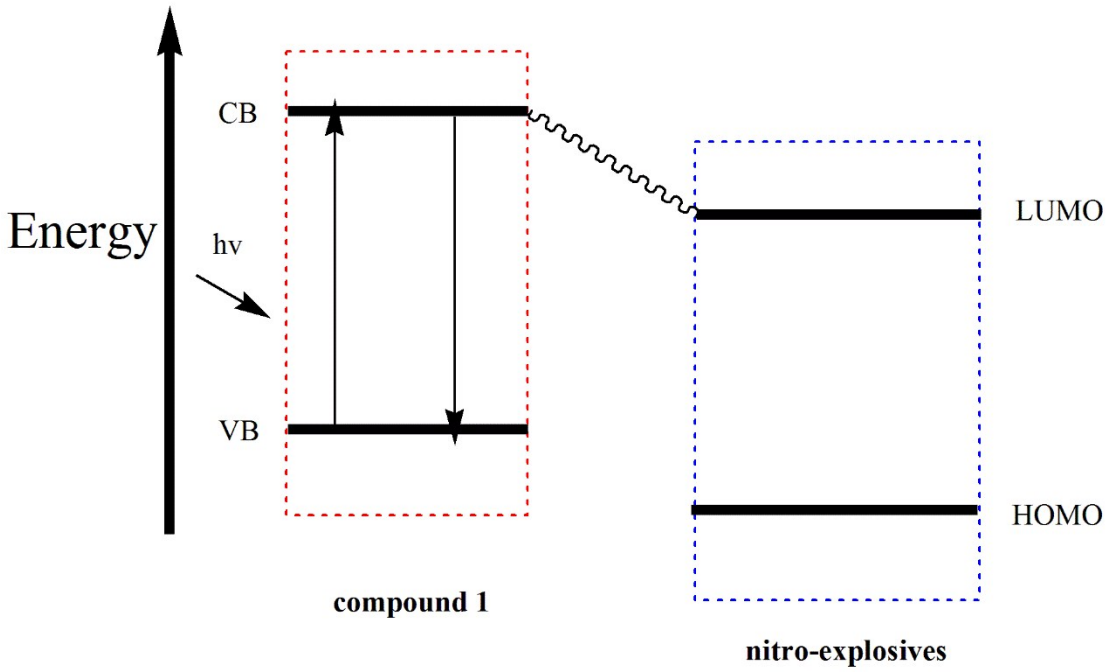

Scheme S2 Schematic illustration of the electron transfer process between **1** and nitro-explosives.

Table S1. Crystal data and structure refinement information for MOF **1**

Crystal system	Monoclinic
Space group	*C* 2/*c*
a, Å	29.018(3)
b, Å	15.7877(16)
c, Å	19.1598(19)
B(°)	107.5170(10)
V, Å ^{3}	8370.6(15)
Z	4
D_{calcd}, g/cm^3	1.095
μ, mm^{-1}	1.467

$F(000)$	2768
θ Range, deg	2.272- 21.128
Reflection collected	33121
Independent reflections (R_{int})	0.0737
Reflections with $I > 2\sigma(I)$	9277
R_1, wR_2 ($I > 2\sigma(I)$)*	0.0694, 0.1862
R_1, wR_2 (all data)**	0.1056, 0.2077

* $R = \sum(F_o - F_c)/\sum(F_o)$, ** $wR_2 = \{\sum[w(F_o^2 - F_c^2)^2]/\sum(F_o^2)^2\}^{1/2}$.

Table S2. Selected bond distances (Å) and angles (°) of structure **1**

Zn1-Zn1A	2.9932(10)	Zn1- O1	2.011(3)
Zn1- O2	2.038(3)	Zn1- O7	2.033(3)
Zn1 O8	2.009(4)	Zn1- O11	1.978(4)
Zn2- O9	1.907(4)	Zn2- O9	1.907(4)
Zn2- O6	2.246(11)	Zn2- O14	1.850(6)
Zn3- Zn3B	2.492(3)	Zn3- O4	2.02(2)
Zn3A-O10	2.141(6)	Zn3B-O14	2.299(5)
Zn3- O5	1.935(6)	Zn3-O14	2.3994(18)
O1- Zn1- Zn1	81.10(10)	O1- Zn1- O2	158.18(14)
O1- Zn1- O7	87.71(15)	O8- Zn1- O7	158.03(16)
O11 -Zn1- Zn1	176.14(12)	O11- Zn1- O7	100.49(17)
O9- Zn2- O9	111.6(2)	O9- Zn-2 O6	96.5(3)
O6- Zn2- O6	171.4(8)	O14- Zn2- O9	124.18(11)
O5- Zn3- Zn3B	148.9(2)	O5- Zn3- O4	108.8(6)

Symmetric codes: (A) x,-1+y,z and (B) x,1+y,z

Table S3. The HOMO-LUMO energies for different analytes other than nitroaromatics.

Analyte	HOMO	LUMO
Nitrobenzene	-7.60	-2.44
Chloroform	-8.60	-1.36
Dichloromethane	-8.42	-0.44
Acetone	-6.64	-0.3
DMF	-6.32	0.99
Acetonitrile	-8.87	1.00
DMSO	-6.05	1.16
Water	-7.94	1.78

iso-propanol	-7.10	2.00
Methanol	-7.21	2.10
THF	-4.20	2.17
DMA	-5.85	2.37
Dioxane	-6.41	2.59

Table S4 Comparison of the selected materials in detective sensitivity for Fe^{3+} ions

Material	Sensitivity	Reference
$Eu(acac)_3@Zn(C_{15}H_{12}NO_2)_2$	5×10^{-3} M	1
$Eu(C_{33}H_{24}O_{12})(H_2NMe)(H_2O)$	2×10^{-4} M	2
$Eu(C_{22}H_{14}O_2)_3$	10^{-4} M	3
$[Eu(BTPCA)(H_2O)]\cdot2DMF\cdot3H_2O$	10^{-5} M	4
MIL-53(Al)	0.9×10^{-6} M	5
$\{[LnCd_2(DTPA)_2(H_2O)_4]\cdot4H_2O$	1.5×10^{-5} M	6
carbon nanoparticles (CNPs)	0.32×10^{-6} M	7
Fluorescent Gold Nanoclusters	5.4×10^{-6} M	8
$[Cd_3(dpa)(DMF)_2(H_2O)_3]\cdot DMF$	1.75×10^{-4} M	9
$Zn_3L_3(DMF)_2$	10^{-5} M	10
$[[Eu_2(MFDA)_2(HCOO)_2(H_2O)_6]\cdot H_2O$	1.0×10^{-4} M	11
$[Tb_4(OH)_4(DSOA)_2(H_2O)_8]\cdot(H_2O)_8$	10^{-6} M	12
1	2.0×10^{-5} M	*In this work*

References:

[1] G. G. Hou, Y. Liu, Q. K. Liu, J. P. Ma and Y. B. Dong, *Chem. Commun.*2011, ***47***, 10731-10733.

[2] S. Dang, E. Ma, Z.M. Sun and H. J. Zhang, *J. Mater. Chem.* 2012, ***22***, 16920-16926.

[3] M. Zheng, H. Q. Tan, Z. G. Xie, L. G. Zhang, X. B. Jing and Z. C. Sun, *ACS Appl. Mater. Interfaces,* 2013, ***5***, 1078-1083.

[4] Q. Tang, S. X. Liu, Y. W. Liu, J. Miao, S. J. Li, L. Zhang, Z. Shi and Z. P. Zheng, *Inorg. Chem.*2013, ***52***, 2799-2801.

[5] C. X. Yang, H. B. Ren and X. P. Yan, *Anal. Chem.*2013, ***85***, 7441-7446.

[6] Q. Liu, F. Wan, L. X. Qiu, Y. Q. Sun and Y. P. Chen, *RSC Adv*., 2014, ***4***, 27013-27021.

[7] K. G. Qu, J. S. Wang, J. S. Ren and X. G. Qu, *Chem. Eur. J.* 2013, ***19***, 7243-7249.

[8] J.-A. A. Ho, H.-C. Chang and W.-T. Su, *Anal. Chem*. 2012, ***84***, 3246-3253.

[9] J. C. Jin, L. Y. Pang, G. P. Yang, L. Hou and Y. Y. Wang, *Dalton Trans*., 2015, ***44***, 17222–17228.

[10] Z. C. Yu, F. Q. Wang, X. Y. Lin, C. M. Wang, Y. Y. Fu, X. J. Wang, Y. N. Zhao and G. D. Li, *J. Solid. State. Chem*., 2015, ***232***, 96-101.
[11] X. H. Zhou, L. Li, H. H. Li, T. Yang and W. Huang, *Dalton Trans*., 2013, **42**, 12403–12409.
[12] X. Y. Dong, R. Wang, J. Z. Wang, S. Q. Zang and T. C. W. Mak, *J. Mater. Chem*. A, 2015, ***3***, 641–647.